Simplified approaches to viscoelastic rolling resistance

Gérard-Philippe Zéhil[a,*], Henri P. Gavin[a]

[a]*Department of Civil and Environmental Engineering, Duke University, 121 Hudson Hall, Box 90287, Research Drive, Durham, NC 27708-0287, United States*

Abstract

Modeling approaches yielding rolling resistance estimates for rigid spheres (and cylinders) on viscoelastic layers of finite thicknesses are introduced as lower-cost alternatives to more comprehensive solution-finding strategies. Detailed examples are provided to illustrate the capabilities of the different approaches over their respective ranges of validity.

Keywords: Rolling resistance, cylinder, sphere, viscoelastic layer, numerical algorithms, simplified approaches, approximate solutions.

1. Content summary

This paper clearly delineates two approaches to estimating the rolling resistance of a rigid sphere on a viscoelastic layer of finite thickness. In both approaches, the effects of slipping friction are neglected.

In the 2D Cylinder-based approach, the sphere is conceptually sliced into a set of cylinders. The rolling resistance incurred by each cylinder is determined by solving a rolling contact problem in two dimensions. The foundation's behavior is described by a numerical compliance in plane strain. The 2D cylinder-based approach builds on results from Qiu (2006) and involves new approximate methods of extending two-dimensional models of rolling cylinders to modeling a rolling sphere in three dimensions. Three numerical methods of varying complexity and accuracy are presented for this approach.

In the direct Fourier series approach, rolling resistance is estimated by computing dissipated power, in the vertical direction, along the contact surface. This approach mainly relies upon the approximate assumption that the stationary vertical stress distribution, as well as the corresponding contact area, are unaltered by motion. Inspired by the recent work of Persson (2010) on rolling resistance, and building upon results from Zéhil and Gavin (2013b,a), as well as on stationary contact results from Jaffar (1988, 1997, 2008), new expressions for the rolling resistance are derived, for different ranges of foundation thickness, in the form of direct Fourier expansions.

2. Introduction and motivation

A full three-dimensional model of a rigid sphere, rolling in steady-state, with or without friction, on a viscoelastic foundation of finite thickness is presented in Zéhil and Gavin (2013b). The candidate contact surface is discretized in a coordinate system that is traveling along with the moving object and the foundation's behavior described using a three-dimensional boundary element formulation, yielding a constitutive model for the layer of the following form

$$\mathbf{CF} = \mathbf{D}, \tag{1}$$

where $\mathbf{F}$ is a nodal surface force vector, $\mathbf{D}$ the corresponding nodal surface displacement vector and $\mathbf{C}$ the foundation's compliance matrix. Full results are then obtained by solving the rolling contact problem at the interface between the rigid sphere and the viscoelastic layer described by equation (1). Efficient means of solving the rolling contact problem are described in Zéhil and Gavin (2013a).

*Corresponding author

Email address: gerard.zehil@duke.edu (Gérard-Philippe Zéhil)

The practical implementation of the full three-dimensional model involves determining matrix $\mathbf{C}$, or at least relevant parts of it, depending on each problem's particular assumptions and goals. Assuming that the candidate contact surface is descretized into K_x and K_y nodes in directions x and y respectively (see figure 1), the total number of nodes is $N_T = K_x K_y$ and the full resulting square compliance matrix $\mathbf{C}$ is of dimension $3N_T = 3K_x K_y$. Taking advantage of existing configurational similarities between pairs of nodes, less than six columns of $\mathbf{C}$ (i.e. about $18K_x K_y$ terms) need to be formed explicitly (see Zéhil and Gavin, 2013b).

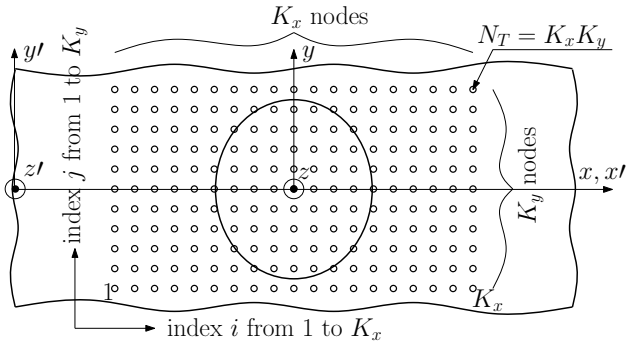

Figure 1: Discretization of the candidate contact surface

In the absence of friction and provided that no horizontal displacements are wanted as part of the solution, only $1/9^{th}$ of the matrix $\mathbf{C}$ is required, from which less than two columns need to be formed explicitly, which adds up to about $2K_x K_y$ terms. This number remains relatively high considering the fact that each matrix entry results from the addition of a sufficient number of terms from a double Fourier series. The computational cost of building compliance matrices increases quadratically with the number of discretization nodes and the truncation order. For reference, in the absence of surface friction, the computational time of building $1/9^{th}$ of a 3D compliance matrix corresponding to $N_T = 41 \times 41 = 1681$ nodes and including $N_{tx} = N_{ty} = 500$ Fourier terms on an Intel® Core™ i7 M620 CPU with 4 MB of cache memory and a clock speed of 2.66 GHz is approximately two minutes. In comparison, solving a frictionless rolling contact problem in 3D, using the same hardware, requires roughly 1.33 seconds. Consequently, the total computational time needed to evaluate the rolling resistance for 23 different values of rolling speed V_s and 15 different values of the applied load P, as we do in sections 3.4 and 4.6 of this manuscript, adds up to almost 54 minutes. This is considered as the reference case.

In many circumstances however, a complete and perfectly accurate solution is not necessary, hence justifying the search for cheaper computational means. This is particularly the case when only an estimate of the rolling resistance is sought. The present work considers alternative approaches to the full three-dimensional model, providing rolling resistance estimates with an accuracy that is suitable for many engineering purposes. According to Qiu (2006), and to Zéhil and Gavin (2013b), the contribution of surface friction to the total rolling resistance is relatively small in comparison with viscoelastic energy dissipation and will therefore be neglected. Experimental evidence strongly supporting this assumption, for the rolling and lubricated sliding of rigid cylinders and spheres on rubber, date back to the 1950's (e.g. Greenwood and Tabor, 1958; Tabor, 1955).

3. 2D cylinder based approaches to a 3D rolling resistance problem

Although configurational similarities afford significant increases of efficiency in three-dimensional solutions, the computational cost remains high in comparison with a similar implementation of a two-dimensional model originally presented by Qiu (2006). We have thus sought approximate solutions for the rolling resistance on a sphere (which is a 3D problem) based on a two-dimensional model of a rolling cylinder.

3.1. Shared principle

The idea is quite simple: a sphere of radius R moving in direction x at a given speed V_s, as depicted in figure 2, is conceptually divided, along the transverse direction y, into an odd number of thin vertical cylindrical elements of

thickness dy, such that one slice is centered in the middle with a symmetrical discretization on both sides. A cylindrical slice whose middle layer is centered at y has radius $R_c(y)$ and penetration $d_c(y)$. In particular, the middle slice is centered at $y = 0$ and its radius $R_c(0)$ is equal to R. The behavior of each cylindrical element is then approached using a two-dimensional model where the underlying subbase is in a state of plane strain (which is where the approximation lies). The vertical load P that is applied to the sphere gets distributed among the cylindrical slices. At equal thickness, the middle slice supports the largest part of the load and thus incurs the largest penetration $d_c(0)$. However, due to the plane stain assumption that is made on the layer in two-dimensions, $d_c(0)$ is typically smaller than the actual penetration of the sphere (d), as determined from a 3D model.

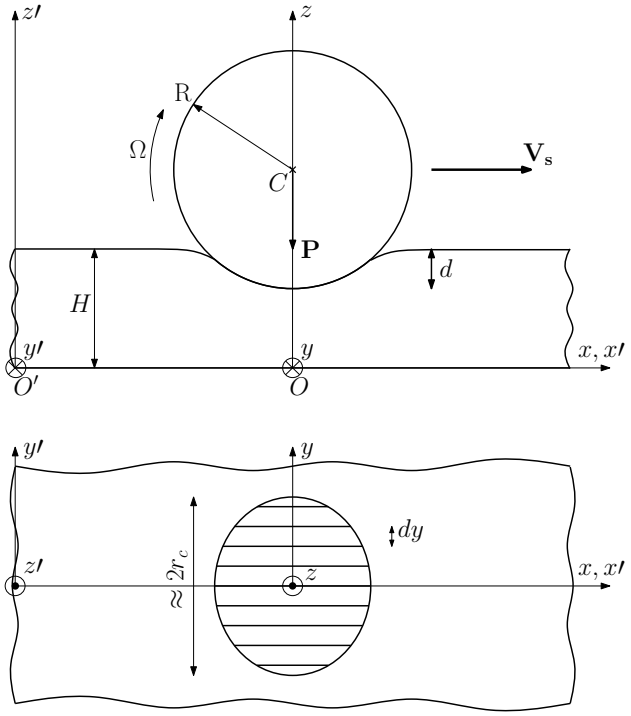

Figure 2: Discretization of the sphere into cylindrical elements (section in plane Oxz and projection on plane Oxy)

The total rolling resistance on the sphere is estimated by summing the rolling resistances incurred by each of its cylindrical elements, taking advantage of symmetry. Three variant algorithms (named "PD", "PP" and "SP") based on these common principles were implemented and tested against 3D results. The additional assumptions specific to each algorithm are presented in the sequel.

3.2. Algorithms PD and PP

3.2.1. Common Core of Algorithms PD and PP

The half-width of the actual contact surface r_c is considered to be roughly equal to the contact radius of a perfectly centered and circular one

$$r_c = \sqrt{d_o(2R - d_o)}, \tag{2}$$

where the penetration of the middle cylindrical slice $d_o = d_c(0)$ is approximated by the vertical distance between the bottom of the sphere and the contact boundary. It is further assumed that the marginal distribution $p_c(y)$ of the total vertical load P, among the cylindrical slices, is quadratic in y, transversally symmetric and continuous at the edges, i.e.

$$p_c(y) = \frac{r_c^2 - y^2}{2R_p}, \tag{3}$$

where R_p is an unknown parameter characterizing the distribution $p_c(y)$ and corresponding to its radius of curvature, at the apex. The equilibrium of vertical forces may be written in analytical form as

$$P = \int_{-r_c}^{+r_c} p_c(y)dy. \tag{4}$$

Plugging (3) into (4) yields the following relation between R_p and r_c

$$r_c^3 = \frac{3}{2}PR_p. \tag{5}$$

Since parameters d_o, r_c and R_p are related by (2) and (5), one of them, say d_o, is chosen to serve as a state variable. The partial load per unit thickness applied to the middle slice $p_c(0)$, may hence be expressed in terms of the state variable d_o as follows

$$p_c(0) = \frac{3P}{4\sqrt{d_o(2R - d_o)}}. \tag{6}$$

Let $p_c^{alg}(d_o)$ be the vertical load per unit length returned by a 2D cylinder-based algorithm for a given penetration d_o of the middle slice. Based on equation (6), the problem is redefined as finding the penetration d_o such that (7) is satisfied

$$p_c^{alg}(d_o) = \frac{3P}{4\sqrt{d_o(2R - d_o)}}. \tag{7}$$

The left-hand-side of equation (7) corresponds to an implicit function of d_o which is evaluated by calling a 2D cylinder-based algorithm. Hence, starting with an initial guess for d_o, successive 2D cylinder-based iterations are performed on the middle slice only, until vertical load equilibrium is achieved.

One way to determine an initial guess for d_o is through an elastic estimate of the contact radius r_c^H, using an analytical result by Hertz (1881), where Poisson's ratio is taken equal to 0.5 and the shear modulus is approximated by the storage modulus $G'(\omega_m)$, where $\omega_m = 2\pi V_s/L_x$ is the angular frequency corresponding to the periodic length L_x in the direction of movement

$$r_c^H = \left(\frac{3PR}{16G'(\frac{2\pi V_s}{L_x})}\right)^{\frac{1}{3}}. \tag{8}$$

3.2.2. Algorithm PD

After d_o has been determined, algorithm PD will enforce geometrical consistency based on the lower profile of the sphere: a cylindrical slice whose middle layer is centered at y is subjected to a penetration $d_c(y)$ given by

$$d_c(y) = d_o - R + \sqrt{R^2 - y^2}. \tag{9}$$

As a result, geometrical consistency is strictly enforced while vertical load equilibrium remains approximate.

3.2.3. Algorithm PP

After d_o has been determined, algorithm PP will enforce vertical load equilibrium based on the applied load P: a cylindrical slice whose middle layer is centered at y is subjected to a vertical load per unit length $p_c(y)$ given by the following equation obtained by combining (2), (3) and (5)

$$p_c(y) = \left(\frac{3P}{4}\right)\left(\frac{d_o(2R - d_o) - y^2}{(d_o(2R - d_o))^{\frac{3}{2}}}\right). \tag{10}$$

Hence conversely, vertical load equilibrium is strictly enforced while geometrical consistency remains approximate.

3.3. Algorithm SP

Algorithm SP makes fewer assumptions and is more computationally involved than algorithms PD and PP, but still within reasonable bounds when compared with the computational cost of 3D results. The previous estimate for the half-width of the contact surface, as given by equation (2), is maintained. However, the assumption pertaining to the marginal transverse distribution of the load (i.e. equation (3)) which previously allowed performing iterations on the middle slice only, is now dropped.

Let $P_c^{alg}(d_o)$ correspond to the total vertical load obtained by adding all partial loads $p_c^{alg}(y)dy$ supported by each cylindrical element when subjected to a penetration $d_c(y)$ given by (9). For the purposes of algorithm SP, the problem is redefined as finding d_o such that $P_c^{alg}(d_o)$ is equal to the applied load P

$$P_c^{alg}(d_o) = \sum \left[p_c^{alg}(y)dy \right] = P. \tag{11}$$

The left-hand-side of equation (11) corresponds to an implicit function of d_o which is evaluated by calling a 2D cylinder-based algorithm as many times as there are slices centered at $y > 0$. Hence, starting with an initial guess for d_o, algorithm SP performs successive 2D cylinder-based iterations involving all cylindrical slices (taking advantage of symmetry), until it finds a global solution satisfying vertical load equilibrium as well as geometrical consistency.

In order to minimize the number of iterations involving multiple cylindrical elements, a good initial guess for d_o is sought by using the common core of algorithms PD and PP.

3.4. Example and results

The performances of algorithms PD, PP and SP are evaluated on the following example: a rigid sphere of radius $R = 2$ cm is rolling at a constant speed V_s, on a viscoelastic foundation of thickness H, under the influence of a horizontal force Q applied at the top, with an intensity such that a steady-state is achieved. The value of Q is therefore not specified. A vertical load P is concomitantly applied at the center of the sphere. The foundation's material is modeled by a three-parameter viscoelastic solid defined by the following master curves

$$\begin{aligned} G'(\omega) &= G_0(1+f)\frac{(1+f)+\omega^2\tau^2}{(1+f)^2+\omega^2\tau^2}, \\ G''(\omega) &= G_0(1+f)\frac{f\omega\tau}{(1+f)^2+\omega^2\tau^2}, \end{aligned} \tag{12}$$

where $G_o = G'(0) = 3.0$ MPa is the static shear modulus, $\tau = 0.25$ s is the creep time and $f = G'(0)/G'(\infty) - 1 = 1$.

Three foundation thicknesses are considered: a relatively thin foundation ($H = 2$ mm), a foundation of intermediate thickness ($H = 5$ mm) and a relatively thick foundation ($H = 30$ mm). For each value of H, the vertical load P and the linear speed V_s are varied over appropriate ranges.

Discretization parameters of two and three-dimensional compliance matrices are set based on practical convergence results presented by Zéhil and Gavin (2013b). The current example setting being an aperiodic one, the spatial periods are set to $L = L_x = L_y = 20$ cm, i.e. large enough to allow for sufficient creep recovery of the viscoelastic foundation between two successive sphere arrivals, at any given point. The nodal spacings retained are $a = a_x = a_y = 0.25$ mm. According to Zéhil and Gavin (2013b, table 1), given the choices for a and L, a Fourier series truncation order of $N_t = 500$ terms is appropriate for the purposes of this work and is therefore adopted.

Regarding algorithms PD, PP and SP, the portion of the sphere that is above the contact surface is sliced into 21 cylindrical divisions. In order to test the level of convergence of these algorithms for $N_t = 500$ terms and 21 cylindrical divisions, tests were performed using a higher truncation order of 2000 terms and as many as 201 cylindrical divisions instead. The corresponding results were found to be well within 0.5% of each other.

Neglecting surface frictions, the rolling resistance estimates given by algorithms PD, PP and SP are plotted against the reference solution resulting from the full three-dimensional model. Furthermore, variations of the mean relative error between the reference solution and its estimate are plotted versus V_s and versus P. Results obtained from the best fitting algorithms are presented in figures 3, 4 and 5, for $H = 2$, 5 and 30 mm respectively. Average computational times for the three algorithms are given in table 1. In the case of reference involving minimal computations for 23 different values of rolling speed and 15 different values of the load, rolling resistance estimates are obtained using

Algorithm	Single run	Reference case	Speed factor
PD	0.21 s	21 s	153
PP	0.18 s	20 s	161
SP	0.56 s	107 s	30

Table 1: Average computational times recorded for algorithms PD, PP and SP. The reference case, including minimal computations for 23 values of V_s and 15 values of P, is compared to a full solution time of 54 minutes (see section 2).

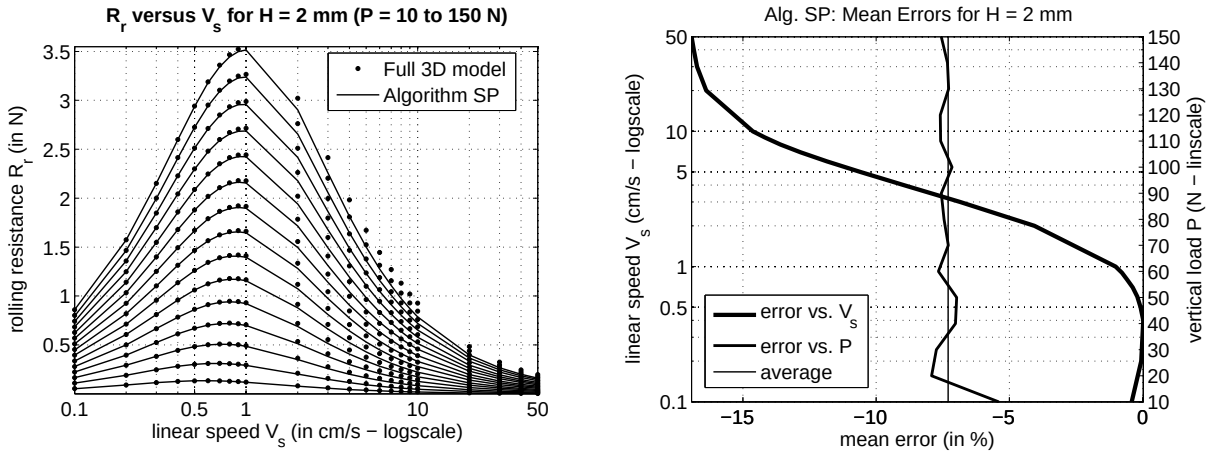

(a) Algorithm SP versus full 3D model

(b) %-errors versus V_s and P

Figure 3: Best results for $H = 2$ mm achieved by Algorithm SP

algorithms PD, PP and SP respectively 153, 161 and 30 times faster than the high fidelity solution given by the full 3D model.

When the foundation strip is relatively thin (i.e. $H = 2$ mm), algorithm SP yields rolling resistance estimates that are the closest to the reference solution given by the full 3D model. Figure 3(b) reveals that the average relative error of algorithm SP over the specified ranges of loading and speed is about -7.3%. Over the same ranges of P and V_s, the average errors of algorithms PP and PD are -9.6% and -27.0% respectively. Hence for relatively thin foundations, the lower computational cost of algorithm PP results in a slightly weaker performance than SP's. However, algorithm PD performs rather poorly in this range of foundation thickness.

Algorithm SP yields the best rolling resistance estimates for foundations of intermediate thickness as well. Its average relative error on the specified ranges of P and V_s is about -3.3% as given by figure 3(b) for $H = 5$ mm. Algorithms PP and PD have average percentage errors of -4.6% and -18.9% respectively, over the same ranges of loading and speed. The ranking of algorithms PP, PD and SP remains the same for thin and intermediate foundation thicknesses, while in both cases, the rolling resistance is mainly approached from below. However, the overall performance of the three algorithms is higher when the foundation is of intermediate thickness.

In the case of thick foundations, algorithm PD performs the best since it overestimates the rolling resistance, on average, by 3.0%, as given by figure 5(b) for $H = 30$ mm, over the specified ranges of loading and speed. In the same conditions, algorithms PP and SP have average relative errors of 9.3% and 9.7% respectively. The performance ranking for thick foundations is hence PD > PP > SP. The same ordering would result if it were based on their computational cost (SP being the most expensive).

Figures 3(b), 4(b) and 5(b) reveal that in all three cases of foundation thickness and regardless of the estimating algorithm, the average percentage error remains rather constant at low rolling velocities then increases (algebraically) with a fairly constant slope (V_s is given on a logarithmic scale) passing through a best performance point (i.e. 0% error) located in the neighborhood of the speed corresponding to the peak of rolling resistance. At higher rolling velocities, the relative error endergoes a change in curvature and tends towards stabilizing.

Alternatively, the error varies less with the vertical loading than the moving speed. For $H = 2$ mm, it oscillates

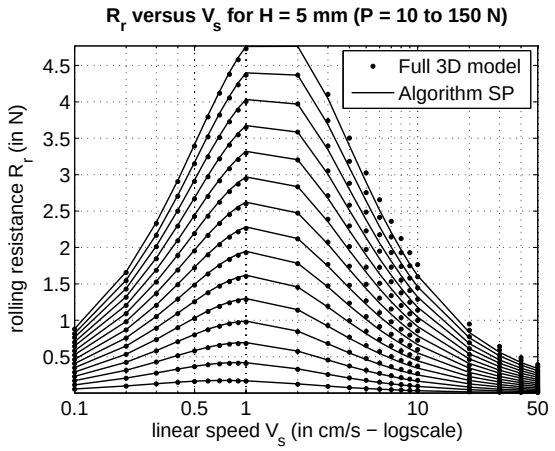

(a) Algorithm SP versus full 3D model

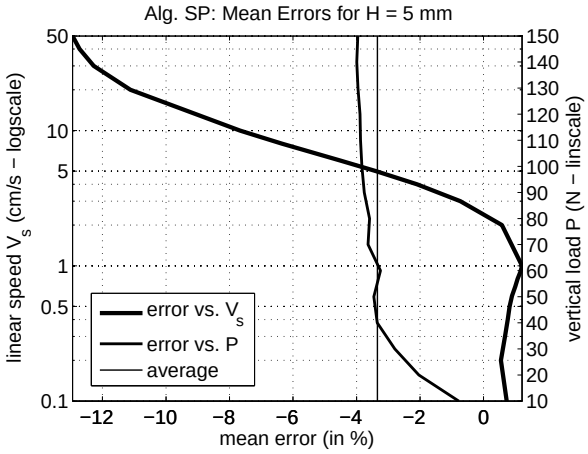

(b) %-errors versus V_s and P

Figure 4: Best results for $H = 5$ mm achieved by Algorithm SP

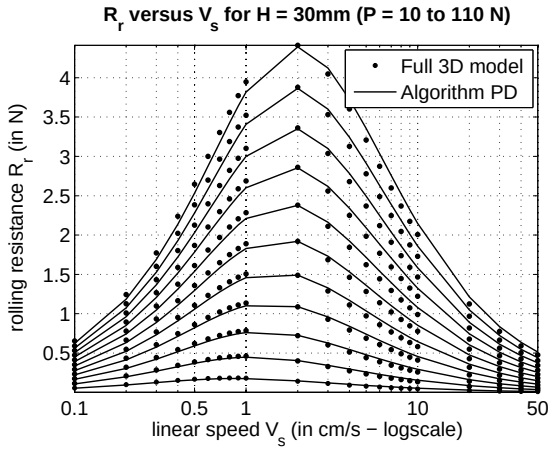

(a) Algorithm PD versus full 3D model

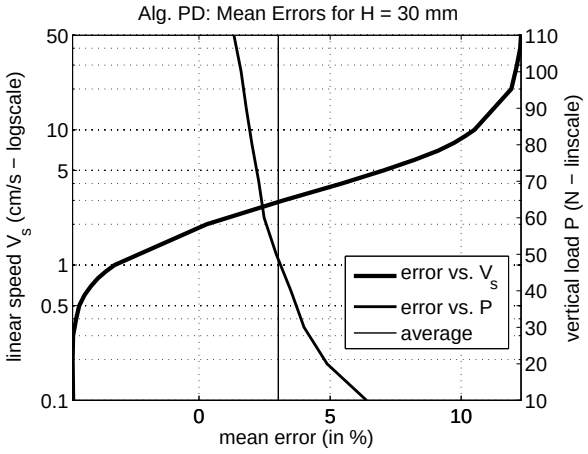

(b) %-errors versus V_s and P

Figure 5: Best results for $H = 30$ mm achieved by Algorithm PD

with a rapidly decreasing amplitude about its global average. For $H = 5$ mm the error slowly increases with the load while behaving oppositely for $H = 30$ mm. In all cases however, it remains fairly close to its global average.

It may be concluded that both algorithms SP and PP yield good rolling resistance estimates for foundations of intermediate thickness (e.g. $H = 5$ mm). Poorer performances are obtained as the foundation thins (e.g. $H = 2$ mm) or thickens (e.g. $H = 30$ mm). The higher computational cost of algorithm SP results in a moderate gain of accuracy in comparison with algorithm PP. Alternatively, algorithm PD yields good rolling resistance estimates for thick foundations (e.g. $H = 30$ mm). In general, the relative error depends less on the loading than it does on the speed. The best performances are obtained in the neighborhood of the moving velocity corresponding to the peak in rolling resistance, which is to the advantage of engineering applications where such a peak is of particular importance.

4. A direct Fourier series approach

4.1. Motivation

Section 3 introduced simplified approaches to estimating the viscoelastic rolling resistance on a sphere at a reduced computational cost as compared to the cost of the full three-dimensional model given in Zéhil and Gavin (2013b). Algorithms PD, PP and SP were based on a transverse summation of two-dimensional rolling cylinder contributions, without further relation to the full 3D model. In the second part of this work, we derive an alternative approach, directly stemming from the full 3D model itself, by introducing simplifying assumptions to it. As we will see, the methodology applies equally to deriving a simplified alternative to the full two-dimensional model of a rolling cylinder presented by Qiu (2006).

The simplified approach developed herein was inspired by the recent works of Persson (2010) and Jaffar (2008), as well as older works by Jaffar (1988, 1997). In Persson's simplified approach to rolling resistance, the effects of viscoelastic dissipation on the contact stress distribution are neglected. Persson's general theory is developed within the mathematical framework of continuous Fourier transforms and results in infinite integral expressions of the rolling resistance involving oscillatory Bessel functions. The method's efficiency hence depends on the practical implementation of such numerical integration. Efficient integration approaches applicable to this type of integrand are discussed for instance by Lucas and Stone (1995). Persson's method is applied to rigid cylinders and spheres rolling on a viscoelastic half-space assuming that the contact stress distribution is of Hertz's form. Alternatively, Jaffar's work provides valuable numerical approaches as well as asymptotic solutions to stationary contact problems between rigid bodies and elastic foundations of finite thickness. Jaffar's work may hence be used, in combination with suitable compliance matrices given by Carbone and Mangialardi (2008); Carbone et al. (2009), to apply Persson's approach to foundations of finite thickness.

Instead, retaining appropriate assumptions, the rolling resistance is directly expressed hereafter in the form of an infinite sum involving Fourier series coefficients of the normal contact stress distribution (i.e. $\sigma_{mn}(z = H)$) as well as Fourier coefficients of the vertical surface displacement field (i.e. $w_{mn}(z = H)$). Using existing equations relating $\sigma_{mn}(z = H)$ to $w_{mn}(z = H)$ from the full 3D boundary element formulation presented in Zéhil and Gavin (2013b), the latter is eliminated yielding an expression of the rolling resistance depending solely on the Fourier series expansion of the normal contact stress. Finally, neglecting the effects of viscoelasticity on $\sigma_z(x, y, z = H)$, it is assumed to keep a stationary elastic profile depending on the foundation thickness, which yields the σ_{mn}'s and hence the rolling resistance.

In comparison with the full 2D and 3D model requirements, the present 'simplified' and 'direct' approach to rolling resistance fully avoids solving the rolling contact problem by making a simplifying assumption on the distribution of normal contact pressure. It also circumvents forming the entire compliance matrix by directly summing terms contributing to the rolling resistance, which constitutes a substantial computational cost reduction. The series furthermore converges very rapidly: for instance, in the example of section 4.6, approximately 99.4% accuracy (with respect to the limit value) is achieved using 50 terms only, for an average computational time of 0.85 seconds. In addition, the method can be implemented in vectorized form to compute the rolling resistance for multiple values of the same parameter: using 50 terms, rolling resistance estimates for 15 different values of the load P are obtained simultaneously for an additional time of 0.14 seconds. The computational time for the reference case including 23 values of V_s and 15 values of P adds up to less than 23 seconds, which is roughly 141 times faster than the full solution (see section 2).

4.2. General Fourier series for the rolling resistance

Let A_c designate the contact area. With appropriate simplifying assumptions[1], a suitable expression of the rolling resistance may be derived from the power associated with vertical stress and displacement fields

$$R_r = \frac{1}{V_s}\iint_{A_c} \sigma_z(x,y,z=H)\frac{\partial w}{\partial t}((x,y,z=H))dxdy, \tag{13}$$

which, given the fact that $\frac{\partial w}{\partial t} = -V_s\frac{\partial w}{\partial x}$ becomes

$$R_r = -\iint_{A_c} \sigma_z(x,y,z=H)\frac{\partial w}{\partial x}(x,y,z=H)dxdy. \tag{14}$$

For shortness of notation we will drop the argument $z = H$ since all quantities are evaluated at the contact interface. Vertical stress and deformation fields are then written in Fourier series as follows

$$\sigma_z(x,y) = \sum_{m_1,n_1=-\infty}^{+\infty} \sigma_{m_1n_1} e^{i\frac{2\pi m_1}{L_x}x} e^{i\frac{2\pi n_1}{L_y}y}, \tag{15}$$

$$w(x,y) = \sum_{m_2,n_2=-\infty}^{+\infty} w_{m_2n_2} e^{i\frac{2\pi m_2}{L_x}x} e^{i\frac{2\pi n_2}{L_y}y}. \tag{16}$$

Differentiating (16) with respect to x we get

$$\frac{\partial w}{\partial x}(x,y) = \sum_{m_2,n_2=-\infty}^{+\infty} i\frac{2\pi m_2}{L_x} w_{m_2n_2} e^{i\frac{2\pi m_2}{L_x}x} e^{i\frac{2\pi n_2}{L_y}y}. \tag{17}$$

Substituting (15) and (17) into (14) and integrating under the summation sign the following expression is obtained

$$R_r = -\sum_{m_1,n_1,m_2,n_2=-\infty}^{+\infty} \left(i\frac{2\pi m_2}{L_x}\sigma_{m_1n_1}w_{m_2n_2}\iint_{A_c} e^{i\frac{2\pi(m_1+m_2)}{L_x}x} e^{i\frac{2\pi(n_1+n_2)}{L_y}y} dxdy \right). \tag{18}$$

Since the vertical stress field $\sigma_z(x,y)$ is equal to zero outside of the contact surface we may integrate on the periodic domain $\left[-\frac{L_x}{2},+\frac{L_x}{2}\right]\times\left[-\frac{L_y}{2},+\frac{L_y}{2}\right]$ using the following result

$$\int_{-\frac{L_x}{2}}^{+\frac{L_x}{2}} e^{i\frac{2\pi(m_1+m_2)}{L_x}x}dx \int_{-\frac{L_y}{2}}^{+\frac{L_y}{2}} e^{i\frac{2\pi(n_1+n_2)}{L_y}y}dy = \begin{cases} 0 & \text{if } (m_1+m_2)(n_1+n_2)=0, \\ L_xL_y & \text{otherwise.} \end{cases} \tag{19}$$

Hence, the only remaining terms in (18) are the ones for which $m_2 = -m_1 \equiv -m$ and $n_2 = -n_1 \equiv -n$. Noting further that $w_{-m-n} = \bar{w}_{mn}$, $\bar{w}_{-mn} = w_{mn}$ and $\sigma_{-mn} = \bar{\sigma}_{mn}$, expression (18) simplifies to

$$R_r = \sum_{m,n=-\infty}^{+\infty} i\left(2\pi m L_y\right)\sigma_{mn}\bar{w}_{mn} = -(4\pi L_y)\sum_{m\geq 1}\left(m\sum_{n=-\infty}^{+\infty} \Im\left(\sigma_{mn}\bar{w}_{mn}\right)\right), \tag{20}$$

where $\Im(z)$ corresponds to the imaginary part of the complex number z.

In Zéhil and Gavin (2013b), we derived the following general solution, relating Fourier coefficients of displacements to Fourier coefficients of surface tractions at the upper boundary of a viscoelastic foundation strip

$$\mathbf{d}_{mn} = \mathbf{T}_{mn,12}\mathbf{T}_{mn,22}^{-1}\mathbf{f}_{mn}, \tag{21}$$

[1]It is assumed that the foundation is subjected to small deformations, in the absence of surface friction, such that surface tractions act in the vertical direction.

where the array quantities were defined as below

$$\begin{aligned}
&\mathbf{d}_{mn} = \langle w_{mn}, u_{mn}, v_{mn} \rangle^T , \\
&\mathbf{f}_{mn} = \left\langle \sigma_{z,mn}, \tau_{xz,mn}, \tau_{yz,mn} \right\rangle^T , \\
&\mathbf{T}_{mn}(z) = \exp(\mathbf{A}_{mn} H).
\end{aligned}$$

$\mathbf{A}_{mn}$ is a complex valued matrix given by

$$\mathbf{A}_{mn} = \begin{bmatrix} 0 & -i\nu_x & -i\nu_y & 0 & 0 & 0 \\ -i\nu_x & 0 & 0 & 0 & G_m^{*^{-1}} & 0 \\ -i\nu_y & 0 & 0 & 0 & 0 & G_m^{*^{-1}} \\ -\rho V_s^2 \nu_x^2 & 0 & 0 & 0 & -i\nu_x & -i\nu_y \\ 0 & \alpha & \gamma & -i\nu_x & 0 & 0 \\ 0 & \gamma & \beta & -i\nu_y & 0 & 0 \end{bmatrix}, \tag{22}$$

where ρ is the material's density, $G_m^* = G'(\omega_m) + iG''(\omega_m)$ is the dynamic shear modulus and the following shorthand parameters have been used

$$\begin{aligned}
&\nu_x = 2\pi m / L_x \; ; \; \nu_y = 2\pi n / L_y, \\
&\beta_x = (4\nu_x^2 + \nu_y^2) G_m^* - \rho V_s^2 \nu_x^2, \\
&\beta_y = (\nu_x^2 + 4\nu_y^2) G_m^* - \rho V_s^2 \nu_x^2, \\
&\beta_{xy} = 3\nu_x \nu_y G_m^*.
\end{aligned} \tag{23}$$

Assuming frictionless contact conditions, we may write $\tau_{xz,mn} = \tau_{yz,mn} = 0$ and thus, regarding the vertical displacement, expression (21) reduces to

$$w_{mn} = T_{mn} \sigma_{mn}, \tag{24}$$

where $\sigma_{z,mn} \equiv \sigma_{mn}$ and T_{mn} is the upper left scalar entry of matrix $\mathbf{T}_{mn,12} \mathbf{T}_{mn,22}^{-1}$ that is, using the unit vector $\mathbf{e}_1 =< 1, 0, 0 >^T$

$$T_{mn} = \mathbf{e}_1^T \mathbf{T}_{mn,12} \mathbf{T}_{mn,22}^{-1} \mathbf{e}_1. \tag{25}$$

Substituting (24) into (20) leads to

$$R_r = (4\pi L_y) \sum_{m \geq 1} \left(m \sum_{n=-\infty}^{+\infty} |\sigma_{mn}|^2 \Im(T_{mn}) \right). \tag{26}$$

Fourier coefficients for the vertical surface traction are given by

$$\sigma_{mn} = \frac{1}{L_x L_y} \int_{-\frac{L_x}{2}}^{+\frac{L_x}{2}} \int_{-\frac{L_y}{2}}^{+\frac{L_y}{2}} \sigma_z(x, y) e^{-i\frac{2\pi m_1}{L_x}} e^{-i\frac{2\pi n_1}{L_y}} dy dx, \tag{27}$$

and may be expressed in polar form as

$$\sigma_{mn} = \frac{1}{L_x L_y} \int_0^{2\pi} \int_0^{r_c} \sigma_z(r, \theta) e^{-iqr\cos\theta} r dr d\theta, \tag{28}$$

where $q = |\mathbf{q}|$, $\mathbf{q} = \left\langle \frac{2\pi m}{L_x}, \frac{2\pi n}{L_y} \right\rangle^T$, $r = |\mathbf{x}|$, $\mathbf{x} = \langle x, y \rangle^T$ and $\theta = \angle(\mathbf{q}, \mathbf{x})$.

Note about cylinders:. the same approach equally applies to the case of a two-dimensional plane strain representation of a rigid cylinder rolling on a viscoelastic foundation of finite thickness. Expression (20) for the rolling resistance, stated per unit cylinder's length, becomes

$$R_r = -4\pi \sum_{m\geq 1} \left[m\Im\left(\sigma_m \bar{w}_m\right)\right], \tag{29}$$

where σ_m and w_m are the complex coefficients of single-variable exponential Fourier series expansions of the vertical traction distribution and displacement field across the foundation's surface. Letting L be the spatial period in one dimension, σ_m is given by

$$\sigma_m = \frac{1}{L}\int_{-\frac{L}{2}}^{+\frac{L}{2}} \sigma_z(x) e^{-i\frac{2\pi m}{L}} dx. \tag{30}$$

The foundation's constitutive equations relating σ_m to w_m were derived by Qiu (2006) in real form and may hence be used to eliminate w_m from (29). The following developments pertain to the case of a sphere knowing that the same principles apply to the cylinder.

4.3. Sphere on a thick foundation

According to Jaffar (2008), in frictionless and stationary conditions, provided that the half-width of the contact area (or equivalently, the contact radius r_c) does not exceed roughly 90% of an elastic foundation's thickness H (i.e. $\gamma = r_c/H \leq 0.9$) the contact pressure distribution keeps Hertz's form, i.e.

$$\sigma_z(r) = \frac{3P}{2\pi r_c^2}\sqrt{1-\left(\frac{r}{r_c}\right)^2}, \tag{31}$$

and the total vertical load P is given by the following expression

$$P = \frac{4\pi E r_c^3}{RD(1-\nu^2)}, \tag{32}$$

where E and ν are Young's modulus and Poisson's ratio respectively and D is defined as follows

$$D = 3\pi + 8\gamma^3\left(b_1 + \frac{2}{5}b_2\gamma^2\right), \tag{33}$$

with coefficients b_m expressed (for $m = 1, 2$) as

$$b_m = \left(-\frac{1}{4}\right)^m \int_0^\infty \left(1 - L(\omega)\right)\omega^{2m} d\omega. \tag{34}$$

For a foundation bonded to its substrate $L(w)$ is given by

$$L(\omega) = \frac{2\kappa\sinh(2\omega) - 4\omega}{2\kappa\cosh(2\omega) + 4\omega^2 + \kappa^2 + 1}, \text{ with } \kappa = 3 - 4\nu. \tag{35}$$

Assuming that (31) and (32) are suitable approximations for steady state moving conditions on a viscoelastic layer, the contact radius may be evaluated by solving (32) for ${r_c}^2$. Following a similar approach to the one presented by Persson (2010), we may further plug (31) into (28) and write

$$\begin{aligned}
\sigma_{mn} &= \frac{1}{L_x L_y}\frac{3P}{2\pi r_c^2}\int_0^{2\pi}\int_0^{r_c} r\sqrt{1-\left(\frac{r}{r_c}\right)^2} e^{-iqr\cos\theta} dr d\theta \\
&= \frac{1}{L_x L_y}\frac{3P}{2\pi r_c^2}\frac{2\pi r_c^2}{(qr_c)^3}\left[\sin(qr_c) - qr_c\cos(qr_c)\right] \\
&= \frac{1}{L_x L_y}\frac{3P}{(qr_c)^3}\left[\sin(qr_c) - qr_c\cos(qr_c)\right].
\end{aligned} \tag{36}$$

[2] in the following section 4.6, the contact radius given by solving (32) for r_c will be designated by r_c^{JK}

Plugging (36) into (26) and using the fact that $T_{m-n} = T_{mn}$ the following expression for the rolling resistance is obtained

$$R_r = 2\pi \frac{(6P)^2}{L_x L_y} \left[\sum_{m,n\geq 1} I_{mn} + \frac{1}{2} \sum_{m\geq 1} I_{m0} \right], \tag{37}$$

where

$$I_{mn} = \frac{m}{L_x} \frac{1}{(qr_c)^6} \left[\sin(qr_c) - qr_c \cos(qr_c) \right]^2 \Im(T_{mn}). \tag{38}$$

4.4. Sphere on a thin foundation

A similar approach to the one presented in section 4.3 may be developed for very thin foundations (i.e. $\gamma \gg 1$) provided that it is based on appropriate estimates of the contact radius and the distribution of normal tractions. Suitable estimates are provided by Jaffar (1997) for the case of a thin elastic foundation in frictionless and stationary conditions.

4.4.1. Thin incompressible foundation

The contact pressure on a thin elastic and incompressible foundation takes the following form

$$\sigma_z(r) = \frac{3P}{\pi r_c^2} \left(1 - \left(\frac{r}{r_c} \right)^2 \right)^2, \tag{39}$$

while (R being the radius of the sphere) the contact radius r_c may be expressed as follows[3]

$$r_c = \left(\frac{96PRH^3}{\pi E} \right)^{\frac{1}{6}}. \tag{40}$$

Plugging (39) into (28) we may write

$$\begin{aligned} \sigma_{mn} &= \frac{1}{L_x L_y} \frac{3P}{\pi r_c^2} \int_0^{2\pi} \int_0^{r_c} r \left(1 - \left(\frac{r}{r_c} \right)^2 \right)^2 e^{-iqr\cos\theta} dr d\theta \\ &= \frac{1}{L_x L_y} \frac{3P}{\pi r_c^2} \frac{16\pi r_c^2}{(qr_c)^3} J_3(qr_c) \\ &= \frac{1}{L_x L_y} \frac{48P}{(qr_c)^3} J_3(qr_c), \end{aligned} \tag{41}$$

where $J_3()$ is the third order Bessel function of the first kind. We may now plug (41) into (26) to get the corresponding expression of the rolling resistance

$$R_r = \frac{2\pi(96P)^2}{L_x L_y} \left[\sum_{m,n\geq 1} I_{mn} + \frac{1}{2} \sum_{m\geq 1} I_{m0} \right], \tag{42}$$

where I_{mn} becomes

$$I_{mn} = \frac{m}{L_x} \frac{1}{(qr_c)^6} J_3^2(qr_c) \Im(T_{mn}). \tag{43}$$

[3] in the following section 4.6, the contact radius given by (45) will be designated by r_c^{JN}

4.4.2. Thin compressible foundation

In the compressible case, the contact pressure on a thin elastic foundation takes the following form

$$\sigma_z(r) = \frac{2P}{\pi r_c^2}\left(1 - \left(\frac{r}{r_c}\right)^2\right), \tag{44}$$

and the contact radius may be expressed as follows

$$r_c = \left(\frac{(1+\nu)(1-2\nu)}{1-\nu}\frac{4RH}{\pi E}\right)^{\frac{1}{4}}. \tag{45}$$

Plugging (44) into (28) we may write

$$\begin{aligned}\sigma_{mn} &= \frac{1}{L_x L_y}\frac{2P}{\pi r_c^2}\int_0^{2\pi}\int_0^{r_c} r\left(1-\left(\frac{r}{r_c}\right)^2\right)e^{-iqr\cos\theta}drd\theta \\ &= \frac{1}{L_x L_y}\frac{2P}{\pi r_c^2}\frac{4\pi}{q^2}J_2(qr_c) \\ &= \frac{1}{L_x L_y}\frac{8P}{(qr_c)^2}J_2(qr_c),\end{aligned} \tag{46}$$

where $J_2()$ is second order Bessel function of the first kind. We may now plug (46) into (26) to get the corresponding expression of the rolling resistance

$$R_r = \frac{2\pi(16P)^2}{L_x L_y}\left[\sum_{m,n\geq 1} I_{mn} + \frac{1}{2}\sum_{m\geq 1} I_{m0}\right], \tag{47}$$

where I_{mn} becomes

$$I_{mn} = \frac{m}{L_x}\frac{1}{(qr_c)^4}J_2^2(qr_c)\mathfrak{I}(T_{mn}). \tag{48}$$

4.5. Foundations of intermediate thickness[4]

To the authors' knowledge, there are no closed form or even approximate analytical expressions of the normal contact pressure between rigid objects and foundation layers of intermediate thicknesses (i.e. for $\gamma = O(1)$ and $\gamma > 0.9$) that may be used at a low computational cost in expression (26) of the rolling resistance, in similar ways to the ones presented in previous sections 4.3 and 4.4.

In axisymmetric problems[5], a numerical strategy, valid for $0 < \gamma < 20$ and Poisson's ratio $0 \leq \nu \leq 0.5$, is detailed by Jaffar (1988): given the indenter's lower profile, a truncated expansion, in modified Legendre polynomials, of the vertical displacement field is written in terms of the unknown penetration d. Integral equations relating the vertical pressure distribution to the vertical displacement field over the contact surface are transformed, using quadrature rules as well as the orthogonality property of modified Legendre polynomials, into a linear system of equations to be solved for the unknown coefficients of a similar truncated expansion of $\sigma_z(r, H)$. The edge condition $\sigma_z(r_c, H) = 0$ yields one additional equation for the unknown penetration d.

The aforementioned system of equations remains linear provided that the contact radius r_c is known, in which case the applied load P is deduced, using vertical force equilibrium, by integrating $\sigma_z(r, H)$ over the contact surface. However, if the vertical load P is given instead, which is practically the case, the system to be solved becomes nonlinear, which increases its numerical cost.

The obtained solution for $\sigma_z(r, H)$, which corresponds to a truncated expansion in terms of modified Legendre polynomials, may then be plugged into (28) yielding similar order truncated expansions of the σ_{mn}'s. The latter can be used in turn in (26) yielding an estimate of the rolling resistance.

[4] unlike the methodologies presented in sections 4.3 and 4.4, the one outlined here was not explicitly implemented and tested by the authors, as part of the present work.

[5] in an axisymmetric context, the radial position is denoted by $r = \sqrt{x^2 + y^2}$

4.6. Example

Let us consider again the case of a rigid sphere, of radius $R = 2$ cm, rolling on a viscoelastic layer of thickness H in similar conditions to the ones described in section 3.4. Three values of H are considered here: $H = 30$ mm and $H = 5$ mm will serve to illustrate the methods behavior over the range of thick foundations, while $H = 10$ μm will allow for checking its accuracy on a very thin layer.

The rolling resistance estimates given by the direct series approach (plain line) are plotted against the reference solution resulting from the full three-dimensional model[6] (round markers) in figure 6(a), for a foundation of thickness $H = 30$ mm. In all cases on figure 6(a), the stationary contact radius remains below 5.15 mm, which corresponds to $\gamma \leq 0.17$ and is therefore well within the thick foundation range. Consequently, the approximate solution closely follows the reference one.

Variations of the mean relative error between the reference solution and its estimate are plotted versus V_s and versus P on figure 6(b). It may be seen that the mean errors remains positive and below 2.8% with a global average of 1.8%. The approximate solution hence approaches the reference one from above, with good accuracy. However, unlike for the 2D cylinder-based approaches presented in section 3, the error depends equally on the loading and the speed: although not monotonically, the mean relative error seems to increase with the vertical load. It first increases than decreases with speed, reaching its 2.8% peak slightly before the peak in rolling resistance. Consequently, the minimum relative error (on the "error vs. V_s" curve) does not seem to occur in the neighborhood of the peak in rolling resistance, as was previously the case.

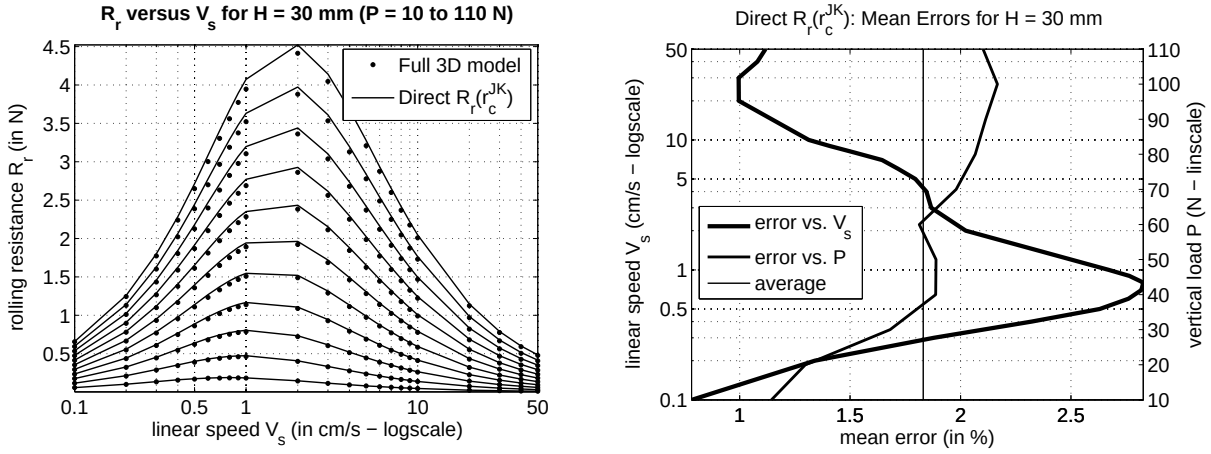

(a) Direct $R_r(r_c^{JK})$ versus full 3D model

(b) %-errors versus V_s and P

Figure 6: Direct approach to R_r versus full 3D model for $H = 30$ mm

Figure 7(a) compares the rolling resistance estimates provided by the direct approach, in the thick foundation range, to the full 3D model reference solution, for $H = 5$ mm. It may be noted that, up to $P = 120$ N, both solutions match extremely well. Starting $P = 130$ N, an increasing gap can be distinguished between the round markers and the plain curves, mainly on the left side of the peak in rolling resistance. In fact, for $P \leq 120$ N, the stationary contact radius remains below 4.87 mm, which corresponds to $\gamma \leq 0.97$ indicating that H is reaching beyond the lower bound of the thick foundation range (section 4.3) into the intermediate range (section 4.5).

Figure 7(b) reveals that the mean relative errors computed over the specified ranges of loading and speed remain below 4.3% with a global average of 0.95%. It can be noted that the "error vs. P" curve crosses the zero error axis at $P = 120$ N and monotonocally increases as greater loads drive γ out of the thick foundation range. The mean relative error remains positive up to $P = 120$ N, which indicates that, over its domain of validity, the simplified approach slightly overestimates the rolling resistance.

[6] without friction

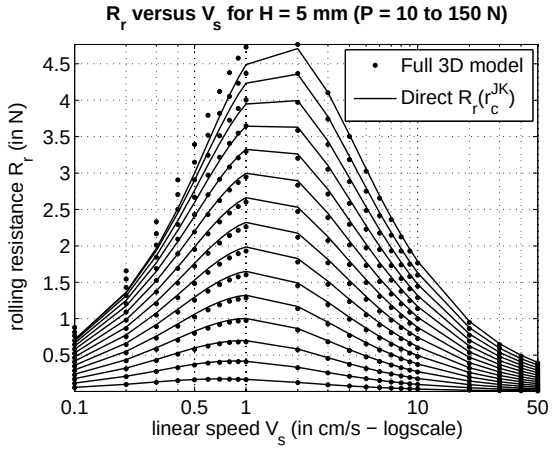

(a) Direct $R_r(r_c^{JK})$ versus full 3D model

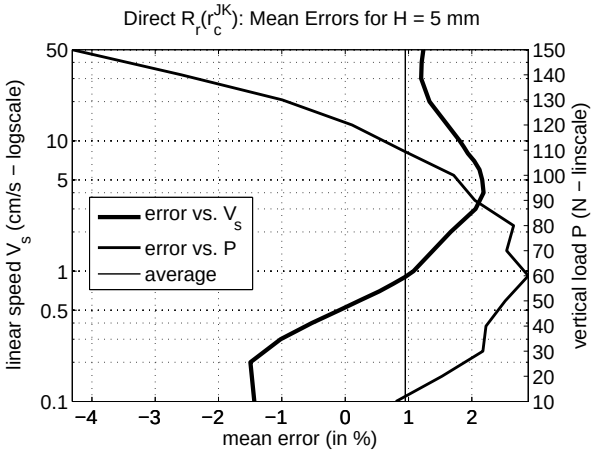

(b) %-errors versus V_s and P

Figure 7: Direct approach to R_r versus full 3D model for $H = 5$ mm

In order to generate a setting whereby $H \ll r_c$ while keeping the 3D model discretization unchanged as well as the same range of linear speed, the layer's thickness is reduced to $H = 10\ \mu$m and the sphere's radius increased to $R = 2000$ m. It is further determined that a suitable loading range corresponds to $0.2 \leq P \leq 2$ kN. Indeed, the associated range of stationary contact radius is $3.33 \leq r_c \leq 4.88$ mm, which is large enough while remaining within the 1×1 cm^2 candidate contact surface. Moreover, the chosen parameters are such that $333 \leq \gamma \leq 488$, which is well within the thin foundation range.

Figure 8(a) indicates that, at the drawing's scale, the rolling resistance estimates given by the direct approach are in perfect agreement with the reference results from the full 3D model. This appears to be true over the entire ranges of loading and speed.

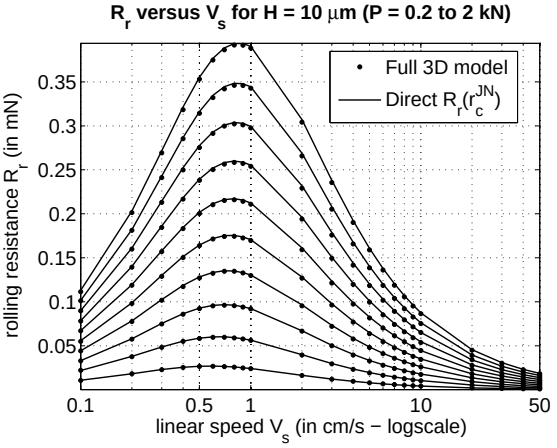

(a) Direct $R_r(r_c^{JN})$ versus full 3D model

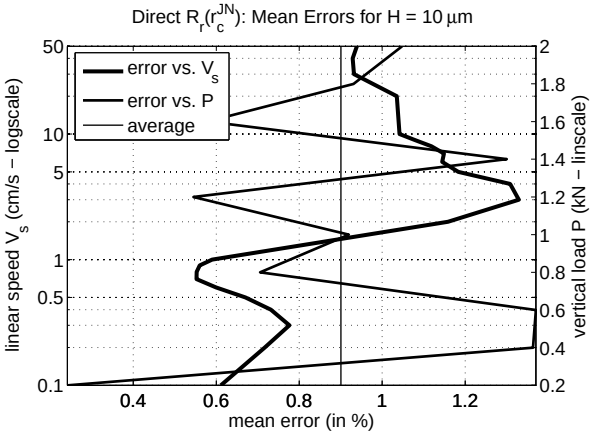

(b) %-errors versus V_s and P

Figure 8: Direct approach to R_r versus full 3D model for $H = 10\ \mu$m

Figure 8(b) reveals that the simplified direct approach very slightly overestimates the rolling resistance. The mean errors remain positive but below 1.4% with a global average of 0.9% which may be considered to be an excellent results.

5. Conclusions

Simplified approaches to the rolling resistance of a rigid sphere on a viscoelastic layer of finite thickness were introduced throughout this work. The method presented in section 4 applies equally to the case of a two-dimensional plane strain representation of a rigid cylinder on a viscoelastic foundation. Although based on simplifying assumptions and therefore yielding approximate rolling resistance estimates, the methods were tested and found to be quite accurate on their respective domains of application. Any comprehensive solution-finding strategy would necessarily involve modeling the viscoelastic layer as well as solving a three-dimensional rolling contact problem between the moving sphere and its foundation, both of which imply conceptual challenges as well as substantial computational costs. In a reference case involving minimal computations for 23 different values of rolling speed and 15 different values of the load, rolling resistance estimates were obtained using algorithms PD, PP, SP and the 'direct' method, respectively 153, 161, 30 and 141 times faster than the high fidelity solution given by the full 3D model of Zéhil and Gavin (2013b). The simplified approaches presented in this work hence constitute quite appealing alternatives in that they provide cheaper rolling resistance estimates of suitable accuracy to many engineering applications.

Acknowledgments

This material is based upon work supported by the National Science Foundation under Grant No. NSF-CMMI-0900324. Any opinions, findings, and conclusions or recommendations expressed in this material are those of the authors and do not necessarily reflect the views of the National Science Foundation.

References

Carbone, G., Lorenz, B., Persson, B., Wohlers, A., 2009. Contact mechanics and rubber friction for randomly rough surfaces with anisotropic statistical properties. The European Physical Journal E 29, 275–284.

Carbone, G., Mangialardi, L., 2008. Analysis of the adhesive contact of confined layers by using a green's function approach. Journal of the Mechanics and Physics of Solids 56 (2), 684–706.

Greenwood, J. A., Tabor, D., 1958. The friction of hard sliders on lubricated rubber: The importance of deformation losses. Proceedings of the Physical Society 71 (6), 989.

Hertz, H., 1881. Über die berührung fester elastischer körper (on contact between elastic bodies). Journal für die reine und angewandte Mathematik 92, 156–171.

Jaffar, M., 1988. A numerical solution for axisymmetric contact problems involving rigid indenters on elastic layers. Journal of the Mechanics and Physics of Solids 36 (4), 401–416.

Jaffar, M., 1997. A general solution to the axisymmetric frictional contact problem of a thin bonded elastic layer. Proceedings of the Institution of Mechanical Engineering 211 (7), 549–558.

Jaffar, M., 2008. On the frictionless axi-symmetric contact of a thick elastic layer and the associated squeeze film problem. Proceedings of the Institution of Mechanical Engineering Part J, Journal of Engineering Tribology 222 (1), 61–68.

Lucas, S., Stone, H., 1995. Evaluating infinite integrals involving bessel functions of arbitrary order. Journal of Computational and Applied Mathematics 64 (11), 217–231.

Persson, B., 2010. Rolling friction for hard cylinder and sphere on viscoelastic solid. The European Physical Journal E Soft Matter 33 (4), 327–33.

Qiu, X., 2006. Full two-dimensional model for rolling resistance: hard cylinder on viscoelastic foundation of finite thickness. Journal of Engineering Mechanics 132 (11), 1241–1251.

Tabor, D., 1955. The mechanism of rolling friction. ii. the elastic range. Proceedings of the Royal Society of London. Series A, Mathematical and PhysicalSciences 229 (1177), 198–220.
URL http://www.jstor.org/stable/99713

Zéhil, G.-P., Gavin, H. P., 2013a. Simple algorithms for solving steady-state frictional rolling contact problems in two and three dimensions. International Journal of Solids and Structures 50 (6), 843 – 852.
URL http://www.sciencedirect.com/science/article/pii/S0020768312004921

Zéhil, G.-P., Gavin, H. P., 2013b. Three-dimensional boundary element formulation of an incompressible viscoelastic layer of finite thickness applied to the rolling resistance of a rigid sphere. International Journal of Solids and Structures 50 (6), 833 – 842.
URL http://www.sciencedirect.com/science/article/pii/S002076831200491X